



# Optimizing supercell structures for Heisenberg exchange interaction calculations

Mojtaba Alaei <sup>1,2,\*</sup> and Artem R. Oganov <sup>1</sup>

<sup>1</sup>*Skolkovo Institute of Science and Technology, Bolshoy Boulevard 30, Building 1, Moscow 121205, Russia*

<sup>2</sup>*Department of Physics, Isfahan University of Technology, Isfahan 84156-83111, Iran*



(Received 21 October 2024; accepted 9 April 2025; published 21 April 2025)

In this paper, we introduce an efficient, linear algebra-based method for optimizing supercell selection to determine Heisenberg exchange parameters from density functional theory (DFT) calculations. A widely used approach for deriving these parameters involves mapping DFT energies from various magnetic configurations within a supercell to the Heisenberg Hamiltonian. However, periodic boundary conditions in crystals constrain the number of extractable exchange parameters. To identify optimal supercell structures for extracting a target number of exchange parameters, we systematically generate supercells within a specified volume range using Hermite normal form matrices. Then, for each supercell, we perform a null space analysis on the coefficient matrix obtained by mapping magnetic configurations to the Heisenberg Hamiltonian. By analyzing the null space results for each supercell structure, we identify the optimal configuration for extracting a target number of exchange parameters. This optimal supercell selection approach significantly reduces computational time and resource requirements. This method, which involves generating and analyzing supercells before performing DFT calculations, has demonstrated a reduction in computational costs by one to two orders of magnitude in many cases.

DOI: [10.1103/PhysRevB.111.144419](https://doi.org/10.1103/PhysRevB.111.144419)

## I. INTRODUCTION

Predicting material properties using theoretical and computational methods is appealing because it reduces the cost of designing materials for specific functions. However, predicting magnetic properties poses unique challenges due to both theoretical and computational difficulties. Theoretically, approximations in electronic structure calculations, especially in density functional theory, often result in inaccurate estimates of electron exchange-correlation energy, leading to incorrect predictions in magnetic systems [1]. Even advanced techniques such as continuum quantum Monte Carlo can be unreliable for comparing magnetic states due to the fixed-node approximation [2]. Computational challenges include long run times and difficulties in achieving electronic convergence, particularly when using large supercells. Therefore, finding an appropriate supercell with fewer atoms can reduce computational cost and may even enable the use of more refined *ab initio* methods [3], such as coupled cluster singles and doubles (CCSD) [4] through density matrix embedding theory (DMET) [5,6].

One common approach for obtaining thermodynamic magnetic properties is to derive a spin model Hamiltonian from electronic structure results, which can then be used to calculate such properties as transition temperatures. There are two main methods for deriving spin models: One involves explicitly calculating interatomic exchange interactions using Green's function methods [7], while the other maps the total energies of different magnetic configurations from electronic structure calculations onto the spin model. This paper focuses

on the latter method, which is applicable to any electronic structure calculation that determines total energy through variational methods.

The main interaction in a spin model Hamiltonian is the Heisenberg exchange interaction, so we assume the Hamiltonian includes only the Heisenberg term. However, including other interactions, such as the Dzyaloshinskii-Moriya (DM) interaction, does not impact the method for determining the optimal supercell presented in this paper. In the mapping method [8], the total energies of various magnetic configurations are used to extract the exchange interactions  $J_{i,j}$  between magnetic moments at sites  $i$  and  $j$  in the Heisenberg term, given by  $-\frac{1}{2} \sum_{i,j} J_{i,j} \hat{\mathbf{S}}_i \cdot \hat{\mathbf{S}}_j$ , where  $\hat{\mathbf{S}}_i$  and  $\hat{\mathbf{S}}_j$  represent the normalized magnetic moment vectors.

For collinear magnetic configurations, where the spin vectors  $\hat{\mathbf{S}}_i$  and  $\hat{\mathbf{S}}_j$  simplify to a single value of  $\pm 1$ , the mapping equation reduces to

$$E_k = \sum_i^m \alpha_{k,i} J_i + c_0. \quad (1)$$

Here,  $k$  denotes the  $k$ th magnetic configuration,  $J_i$  represents the exchange interaction for the  $i$ th nearest neighbor, and  $E_k$  is the total energy obtained from electronic structure calculations for that magnetic configuration. The term  $c_0$  is a constant. The coefficients  $\alpha_{k,i}$  and  $c_0$  form a matrix  $\mathbb{A}_{n \times m+1}$ , where  $n$  is the number of different magnetic configurations. From this matrix, one can determine, for a given supercell, up to which neighbor the exchange interactions can be reliably calculated [1].

To visually demonstrate the limitations of calculating exchange interactions in a supercell, we consider a  $2 \times 2$  hexagonal monolayer supercell containing four magnetic

\*Contact author: m.alaei@skoltech.ru; m.alaei@iut.ac.ir

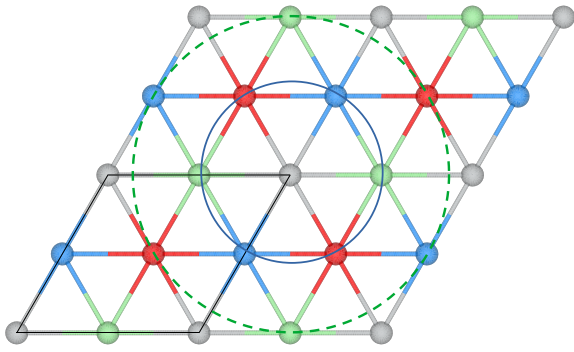


FIG. 1. The figure illustrates the effect of periodic boundary conditions on Heisenberg exchange calculations. It shows a  $2 \times 2$  supercell of a hexagonal monolayer, where each of the four atoms in the supercell is represented by a distinct color, indicating different magnetic directions. As shown, the colors for the first nearest neighbors (inner circle) and second nearest neighbors (outer circle) are identical. This demonstrates that the exchange interactions between the first and second neighbors cannot be computed in this supercell using the mapping method, as they share the same  $\alpha$  coefficient [Eq. (1)].

atoms, as shown in Fig. 1. Each atom is assigned a distinct color to represent an independent magnetic direction. However, due to periodic boundary conditions, these colors repeat, leading to a situation where the first and second nearest neighbors share the same set of distinct colors. This implies that the coefficients  $\alpha_{k,1}$  and  $\alpha_{k,2}$  are identical, making it impossible to independently determine the exchange interactions  $J_1$  and  $J_2$  in this supercell.

In more complex systems, this limitation may not be as easily detected, so a mathematical approach is necessary. By applying Gaussian elimination and analyzing the null space of matrix  $A$ , we derive a general relationship,  $\alpha_{k,l} = \beta_0 + \sum_{i<l} \beta_i \alpha_{k,i}$ , which shows that  $J_l$  depends on the preceding exchange interactions  $J_{i<l}$  due to periodic boundary conditions. To calculate exchange interactions beyond the  $l$ th nearest neighbor, either a larger supercell or a supercell with a different shape is required [see the Supplemental Material (SM) [9]].

To calculate exchange interactions up to a specific number of nearest neighbors, identifying the smallest supercell that permits the computation of these interactions can significantly reduce computational costs. Researchers typically extend the primitive cell by integer factors  $n$ ,  $m$ , and  $q$  to form a conventional  $n \times m \times q$  supercell. However, generating supercell structures can be more generally achieved using a  $3 \times 3$  transformation matrix. By applying all possible transformations (up to a specific supercell size), one can explore the supercell space and identify the optimal supercell structure for calculating the desired exchange interactions.

In this paper, we present a computational method for efficiently identifying supercell structures that meet the desired criteria. In the following sections, we provide a detailed explanation of our approach for selecting the optimal supercell structures. Next, we demonstrate the computational time savings achieved with this method using specific examples. Finally, we present a practical example of applying density functional theory (DFT) with the optimal

supercell structures to calculate the exchange parameters of  $\text{Fe}_2\text{O}_3$ .

## II. METHOD

### A. Building supercell structures

To construct a supercell from a parent cell, we can use an integer matrix  $\mathbb{H}$  to transform the parent lattice vectors  $\mathbb{V}_p$  into the supercell lattice vectors  $\mathbb{V}_s$  using  $\mathbb{V}_s = \mathbb{H} \mathbb{V}_p$ . The lattice vectors are represented in rows in both  $\mathbb{V}_s$  and  $\mathbb{V}_p$ . To generate supercell structures for a specific size  $n$ , we use Hermite normal form (HNF) matrices to transform the parent lattice and then apply rotational symmetry of the lattice to eliminate duplicate supercells. It has been shown that all possible HNF matrices can be created in an upper-triangular form [10–12],

$$\mathbb{H} = \begin{bmatrix} a & b & c \\ 0 & d & e \\ 0 & 0 & f \end{bmatrix}, \quad 0 \leq b < d, \quad 0 \leq c, e < f, \quad (2)$$

where  $a, \dots, f$  are integers. In addition to the inequality constraints, the size  $n$  of the supercell dictates the determinant of the matrix ( $|\mathbb{H}| = a \times d \times f = n$ ). Using these constraints, all possible combinations of  $a, \dots, f$  can be identified [12,13]. When  $b = c = e = 0$ , the HNF matrix generates a conventional supercell.

However, relying solely on the HNF matrix transformation may result in superlattices with lattice vectors that differ greatly in length, making them impractical. Minkowski reduction [14,15] helps to address this issue by providing shorter, more orthogonal lattice vectors without altering the lattice volume. Therefore, in this work, we apply Minkowski reduction after performing the HNF matrix transformation.

### B. Finding optimal supercell structures

For each magnetic configuration (e.g.,  $k$ th), within a supercell, the total energy of the electronic structure is related to exchange interactions by Eq. (1). For  $n$  magnetic configurations, we can represent this relationship using the following linear algebra equation ( $\mathbb{A}\mathbb{J} = \mathbb{E}$ ):

$$\begin{pmatrix} 1 & \alpha_{1,1} & \alpha_{1,2} & \cdots & \alpha_{1,m} \\ 1 & \alpha_{2,1} & \alpha_{2,2} & \cdots & \alpha_{2,m} \\ 1 & \alpha_{3,1} & \alpha_{3,2} & \cdots & \alpha_{3,m} \\ \vdots & \vdots & \vdots & \ddots & \vdots \\ 1 & \alpha_{n,1} & \alpha_{n,2} & \cdots & \alpha_{n,m} \end{pmatrix} \begin{pmatrix} J_1 \\ J_2 \\ \vdots \\ J_m \end{pmatrix} = \begin{pmatrix} E_1 \\ E_2 \\ E_3 \\ \vdots \\ E_n \end{pmatrix}. \quad (3)$$

By using Gaussian elimination to find the reduced row echelon form (RREF) of matrix  $\mathbb{A}$  and identifying null space vectors [16], we can determine which columns depend on earlier columns. This tells us the maximum distance (nearest neighbor) for calculating exchange interactions. For example, if the column for the  $q$ th nearest neighbor (column  $q + 1$ ) is the first one that depends on previous columns, we should set  $J_{i \geq q} = 0$  to avoid incorrect results due to this dependency. To include exchange interactions beyond the  $q$ th nearest neighbor, a larger supercell is needed. Note that the rank of matrix  $\mathbb{A}$  may not depend on the index of the first dependent column. This occurs because, in some cases, columns following the first dependent column may be linearly independent on

the preceding columns (we have provided an example in the SM to clarify this issue [9]). As a result, the rank of the matrix can exceed  $q$ . Therefore, focusing solely on rank can be misleading when determining the limitations of a supercell.

To search for the optimal supercell for maximizing the number of exchange interactions within a range of sizes, the following simplified steps can be applied: (1) Generate supercell structures using HNF matrices, then apply Minkowski reduction. (2) Create random magnetic configurations for each supercell and construct the  $\mathbb{A}$  matrix. (3) Use Gaussian elimination to find the null space vectors of matrix  $\mathbb{A}$  and identify the first dependent column. (4) Sort the supercells based on the index of the first dependent column.

We have two options in step (2): Use random or generate all possible linear magnetic configurations. However, the total number of configurations increases exponentially as the number of magnetic atoms increases, which makes the random approach more practical. When constructing matrix  $\mathbb{A}$ , we remove duplicate rows, as duplicates can arise in small supercells due to symmetry or repeated configurations. It is advisable to avoid using such small supercells, as they reduce the number of unique magnetic configurations required to calculate exchange parameters. Therefore, the fraction of distinct configurations can also guide the selection of an optimal supercell.

We can extend the method to a more general Hamiltonian,  $-\frac{1}{2} \sum_{i,j} \sum_{\alpha,\beta} \mathcal{J}_{i,j}^{\alpha\beta} S_i^\alpha S_j^\beta$ , where  $S_i^\alpha$  and  $S_j^\beta$  represent the components of magnetic moments along the  $\alpha$  and  $\beta$  directions (i.e.,  $x$ ,  $y$ , and  $z$ ). The tensor  $\mathcal{J}_{i,j}$  includes three types of interactions: Heisenberg ( $J_{ij} = \frac{1}{3} \text{Tr} \mathcal{J}_{ij}$ ), DM [ $D_{ij} = \frac{1}{2} (\mathcal{J}_{ij} - \mathcal{J}_{ij}^T)$ ], and anisotropic exchange tensor [ $\Gamma_{ij} = \frac{1}{2} (\mathcal{J}_{ij} + \mathcal{J}_{ij}^T) - J_{ij} \mathbb{1}$ ]. The non-Heisenberg interactions originate from spin-orbit coupling and can lead to noncollinear magnetic ordering phenomena, such as skyrmions [17,18]. For each pair of  $\alpha$  and  $\beta$ , we can construct a coefficient matrix and perform a null space analysis on it. The results of the null space analysis are influenced by the superlattice structure. Therefore, we anticipate that the null space analysis of this Hamiltonian—which is a generalized version of the Heisenberg Hamiltonian—will align with the findings from the analysis of the standard Heisenberg Hamiltonian.

We have made a code available on GitHub [19] that can generate optimal structures within a specified volume range. The code requires only a parent cell (e.g., a primitive cell) to find the best supercell structures. It is written in PYTHON, and is both parallelized and efficient.

### III. RESULTS AND DISCUSSIONS

To demonstrate the results of our method, we use a  $\text{CrCl}_3$  monolayer as an example (see Fig. 2). We generate supercell sizes ranging from 1 to 16 using HNF matrices. These numbers (1–16) indicate how many times larger the volume of the supercell structure is compared to the original (parent) structure. Applying the algorithm leads us to a supercell size of 8, which allows us to calculate exchange parameters up to the eighth nearest neighbors. In contrast, using conventional supercell construction, we would need a  $4 \times 4$  supercell (size

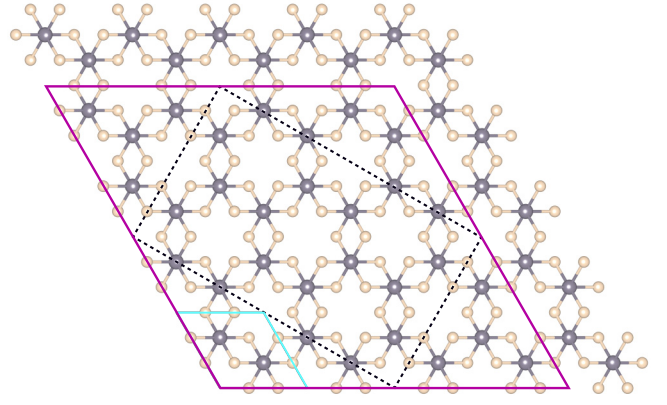


FIG. 2. The figures illustrate different cell sizes of  $\text{CrCl}_3$ . Larger spheres represent Cr atoms, while smaller spheres represent Cl atoms. Cyan lines outline the primitive cell, purple lines indicate a  $4 \times 4$  supercell (size 16), and dashed lines mark a supercell of size 8. Both supercells allow for calculating the Heisenberg exchange interaction up to the eighth nearest neighbor. However, the larger supercell (size 16) requires approximately eight times more computational time compared to the supercell of size 8.

16) to calculate the same exchange parameters. This results in an approximately eightfold reduction in computational time for methods such as DFT, which scale as  $n^3$ , where  $n$  is the number of electrons.

Table I presents several examples that highlight the method's efficiency. As shown in the table, this approach can speed up calculations by nearly an order of magnitude in many cases. According to Table I, the method becomes significantly more efficient when the goal is to calculate exchange interactions at greater distances. Among the materials listed in Table I, we chose  $\text{Fe}_2\text{O}_3$  to showcase the effectiveness of our method in finding an optimal supercell for calculating exchange interactions. When generating supercell structures with sizes ranging from 1 to 12, we obtain 322 distinct structures for  $\text{Fe}_2\text{O}_3$ . Figure 3 displays the maximum number of nearest neighbors that can

TABLE I. The table presents examples of magnetic materials to compare our method for finding the optimal supercell with the conventional method. The primitive cells of NiO, MnTe,  $\text{Fe}_2\text{O}_3$ , and  $\text{MnO}_2$  contain 2, 2, 4, and 2 magnetic atoms, respectively. The table also indicates the number of allowed exchange interactions for each optimal supercell size, along with the equivalent conventional supercell that can be used to calculate the same number of exchange interactions.

Material	Conventional supercell size	Permitted $J_n$	Optimal supercell size	Speedup
NiO	8 ( $2 \times 2 \times 2$ )	$J_1 \cdots J_5$	5	$\sim 4$
	27 ( $3 \times 3 \times 3$ )	$J_1 \cdots J_7$	7	$\sim 57$
MnTe	18 ( $3 \times 3 \times 2$ )	$J_1 \cdots J_7$	8	$\sim 11$
	48 ( $4 \times 4 \times 3$ )	$J_1 \cdots J_{13}$	12	$\sim 64$
$\text{Fe}_2\text{O}_3$	8 ( $2 \times 2 \times 2$ )	$J_1 \cdots J_{12}$	4	$\sim 8$
	27 ( $3 \times 3 \times 3$ )	$J_1 \cdots J_{22}$	8	$\sim 38$

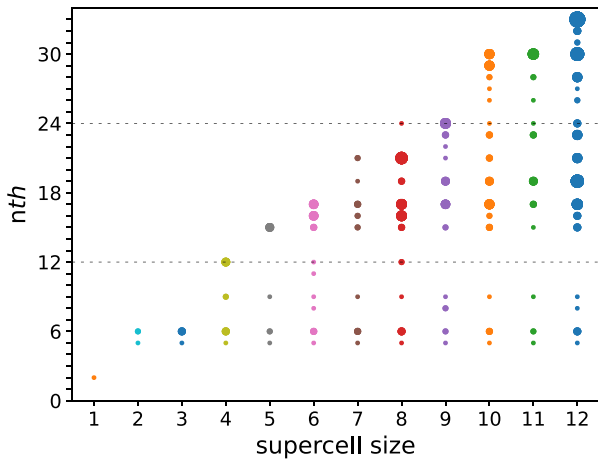


FIG. 3. The plot shows the allowed exchange interactions for supercell structures generated with supercell sizes ranging from 1 to 12. The  $x$  axis represents different supercell sizes, while the  $y$  axis indicates the number of permitted exchange interactions for each supercell structure. Each color indicates the data associated with a specific supercell size. For each supercell size, there are multiple distinct supercell structures. For example, at supercell size 8, there are 42 distinct supercell structures. The size of the circles in the plot reflects the population of structures that allow the calculation of a specific number of exchange interactions for these supercell structures. The data used to generate this plot can be found in Table S2 of the SM [9].

be considered for each supercell structure in an *ab initio* calculation. As shown, different structures allow varying numbers of nearest neighbors for each supercell size. Since the supercell size primarily influences the computation time, it is recommended to choose the structure with the highest number of permitted nearest neighbors for more efficient calculations.

According to Table I and the plot in Fig. 3, a supercell structure of size 4 can be used to compute exchange interactions up to  $J_{12}$ . This structure, along with the other  $\text{Fe}_2\text{O}_3$  supercell structure, is visualized in Fig. 4. Using the least-squares method, we fit DFT results from 48 distinct magnetic configurations within this supercell to the Heisenberg Hamiltonian, yielding exchange interactions up to  $J_{12}$ , as shown in Fig. 5. The significant values of  $J_{11}$  and  $J_{12}$  suggest that interactions beyond  $J_{12}$  may be relevant, indicating the need for a larger supercell for accurate calculation.

As shown in Fig. 3, a supercell structure of size 8 (visualized in Fig. 4) allows for the calculation of exchange interactions up to  $J_{24}$ . In contrast, a conventional supercell of the same size ( $2 \times 2 \times 2$ ) only permits calculations up to  $J_{12}$  (see Table I). According to Table I, a conventional supercell larger than  $3 \times 3 \times 3$  would be necessary to compute interactions up to  $J_{24}$ , underscoring the importance of selecting an optimal supercell structure.

With the new supercell structure of size 8, we observe that the value of  $J_{10}$  differs significantly from those obtained using the size 4 supercell. Additionally, we find notable values for  $J_{13}$  (Fig. 5). Beyond the 13th nearest neighbor, the exchange interactions approach zero, suggesting that interactions up

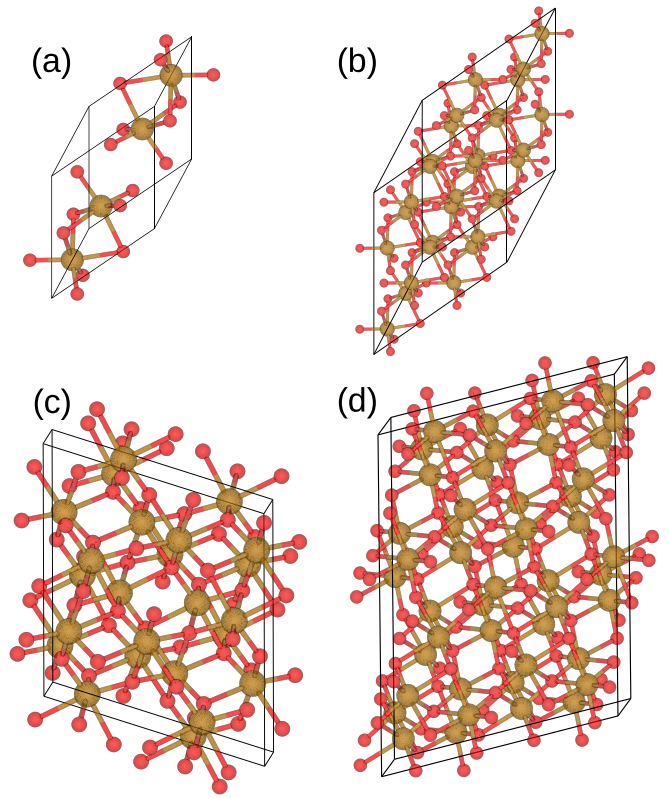


FIG. 4. The figure shows the primitive and supercell structures of  $\text{Fe}_2\text{O}_3$ . (a) represents the primitive cell, (b) illustrates the conventional  $2 \times 2 \times 2$  supercell, (c) displays the supercell structure of size 4, which allows the calculation of exchange interactions up to  $J_{12}$ , and (d) shows the supercell structure of size 8, which permits the calculation of exchange interactions up to  $J_{24}$ . The small spheres represent oxygen atoms, while the large spheres represent iron atoms.

to  $J_{13}$  are sufficient for accurate modeling. Thus, using the size 8 supercell derived from our algorithm, we can compute exchange interactions up to  $J_{24}$ . In contrast, the conventional  $2 \times 2 \times 2$  supercell only resolves interactions up to  $J_{12}$ , where

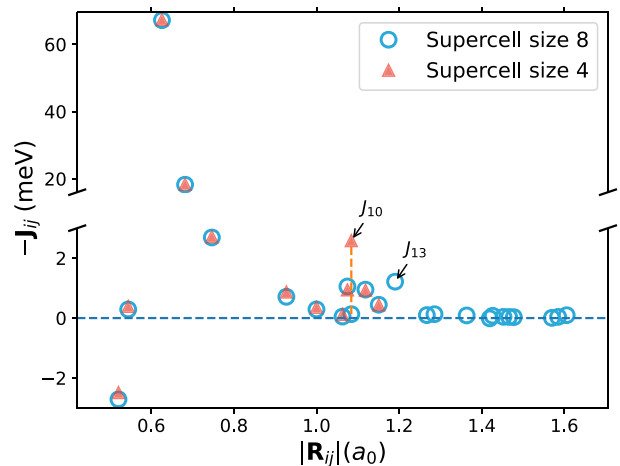


FIG. 5. The plot presents DFT results for two supercell structures of  $\text{Fe}_2\text{O}_3$ , one with a size of 4 and the other with a size of 8. Using the structure of size 4, we can calculate Heisenberg exchange interactions up to  $J_{12}$ . However, with a supercell of size 8, we can estimate exchange parameters up to  $J_{24}$ .



ambiguities remain, as  $J_{10}$ ,  $J_{11}$ , and  $J_{12}$  still exhibit significant values, suggesting that interactions beyond  $J_{12}$  may still play a role.

To investigate the impact of including exchange interactions beyond  $J_{12}$ , we calculated the transition temperature using Monte Carlo simulations with the ESpinS code [20]. When using exchange interactions derived from supercell size 4, the transition temperature is 780 K, whereas using interactions from supercell size 8 yields a transition temperature of 805 K. This difference highlights the significance of considering longer-range interactions. For further details, please refer to the SM [9].

#### IV. CONCLUSION

In this paper, we introduced a method to identify optimal supercell structures for calculating exchange interactions by

mapping spin-polarized *ab initio* results onto the Heisenberg Hamiltonian. This method can significantly accelerate exchange interaction calculations, often by an order of magnitude. It is particularly beneficial for *ab initio* methods with convergence challenges, such as meta-generalized gradient approximation (GGA) methods [21,22]. By selecting the smallest possible supercell, convergence issues are mitigated, especially in spin-polarized calculations, where these challenges are typically more pronounced.

#### ACKNOWLEDGMENTS

M.A. thanks Nafiseh Rezaei for her valuable comments and assistance in improving Figs. 1 and 2. This work has been supported by the Russian Science Foundation (Grant No. 19-72-30043).

- 
- [1] Z. Mosleh and M. Alaei, Benchmarking density functional theory on the prediction of antiferromagnetic transition temperatures, *Phys. Rev. B* **108**, 144413 (2023).
- [2] R. J. Needs, M. D. Towler, N. D. Drummond, and P. L. Ríos, Continuum variational and diffusion quantum Monte Carlo calculations, *J. Phys.: Condens. Matter* **22**, 023201 (2010).
- [3] G. H. Booth, A. Grüneis, G. Kresse, and A. Alavi, Towards an exact description of electronic wavefunctions in real solids, *Nature (London)* **493**, 365 (2013).
- [4] J. Čížek, On the correlation problem in atomic and molecular systems. Calculation of wavefunction components in Ursell-type expansion using quantum-field theoretical methods, *J. Chem. Phys.* **45**, 4256 (1966).
- [5] G. Knizia and G. K.-L. Chan, Density matrix embedding: A simple alternative to dynamical mean-field theory, *Phys. Rev. Lett.* **109**, 186404 (2012).
- [6] Z.-H. Cui, T. Zhu, and G. K.-L. Chan, Efficient implementation of *ab initio* quantum embedding in periodic systems: Density matrix embedding theory, *J. Chem. Theory Comput.* **16**, 119 (2020).
- [7] A. Szilva, Y. Kvashnin, E. A. Stepanov, L. Nordström, O. Eriksson, A. I. Lichtenstein, and M. I. Katsnelson, Quantitative theory of magnetic interactions in solids, *Rev. Mod. Phys.* **95**, 035004 (2023).
- [8] A. Sadeghi, M. Alaei, F. Shahbazi, and M. J. P. Gingras, Spin Hamiltonian, order out of a Coulomb phase, and pseudocriticality in the frustrated pyrochlore Heisenberg antiferromagnet  $\text{FeF}_3$ , *Phys. Rev. B* **91**, 140407(R) (2015).
- [9] See Supplemental Material at <http://link.aps.org/supplemental/10.1103/PhysRevB.111.144419> for additional data, including details on the supercell optimization process using  $\text{CrCl}_3$ , explanations of Hermite Normal Form matrices, Minkowski reduction, and Reduced Row Echelon Form, as well as exchange interaction calculations and Monte Carlo simulations for  $\text{Fe}_2\text{O}_3$ .
- [10] A. Santoro and A. D. Mighell, Coincidence-site lattices, *Acta Crystallogr. Sect. A* **29**, 169 (1973).
- [11] A. Santoro and A. D. Mighell, Properties of crystal lattices: the derivative lattices and their determination, *Acta Crystallogr. Sect. A* **28**, 284 (1972).
- [12] G. L. W. Hart and R. W. Forcade, Algorithm for generating derivative structures, *Phys. Rev. B* **77**, 224115 (2008).
- [13] G. L. W. Hart and R. W. Forcade, Generating derivative structures from multilattices: Algorithm and application to hcp alloys, *Phys. Rev. B* **80**, 014120 (2009).
- [14] P. Q. Nguyen and D. Stehlé, Low-dimensional lattice basis reduction revisited, *ACM Trans. Algorithms* **5**, 1 (2009).
- [15] M. Bremner, *Lattice Basis Reduction* (CRC Press, New York, 2011).
- [16] K. Singh, *Linear Algebra: Step by Step* (Oxford University Press, Oxford, UK, 2013).
- [17] Y. Tokura and N. Kanazawa, Magnetic skyrmion materials, *Chem. Rev.* **121**, 2857 (2021).
- [18] A. Ghojavand, M. Soenen, N. Rezaei, M. Alaei, C. Sevik, and M. V. Milošević, Strain-tunable magnetic and magnonic states in Ni-dihalide monolayers, *Phys. Rev. Mater.* **8**, 114401 (2024).
- [19] <https://github.com/malaei/SUPERHEX/>.
- [20] N. Rezaei, M. Alaei, and H. Akbarzadeh, ESpinS: A program for classical Monte-Carlo simulations of spin systems, *Comput. Mater. Sci.* **202**, 110947 (2022).
- [21] J. Sun, A. Ruzsinszky, and J. P. Perdew, Strongly constrained and appropriately normed semilocal density functional, *Phys. Rev. Lett.* **115**, 036402 (2015).
- [22] J. W. Furness, A. D. Kaplan, J. Ning, J. P. Perdew, and J. Sun, Accurate and numerically efficient  $r^2\text{SCAN}$  meta-generalized gradient approximation, *J. Phys. Chem. Lett.* **11**, 8208 (2020).